Agricultural and Forest Meteorology xxx (2016) xxx–xxx

Contents lists available at ScienceDirect

Agricultural and Forest Meteorology

journal homepage: www.elsevier.com/locate/agrformet

# Carbon and energy flux from a *Phragmites australis* wetland in Zhangye oasis-desert area, China

Qiang Zhang[a,b,c], Rui Sun[a,b,c,*], Guoqing Jiang[a,b,c], Ziwei Xu[a,b,c], Shaomin Liu[a,b,c]

[a] *State Key Laboratory of Remote Sensing Science, Jointly Sponsored by Beijing Normal University and the Institute of Remote Sensing Applications, CAS, Beijing 100875, China*
[b] *School of Geography and Remote Sensing Sciences, Beijing Normal University, Beijing 100875, China*
[c] *Beijing Key Lab for Remote Sensing of Environment and Digital Cities, Beijing 100875, China*

ARTICLE INFO

*Article history:*
Received 30 August 2015
Received in revised form
23 December 2015
Accepted 25 February 2016
Available online xxx

*Keywords:*
Carbon flux
Energy flux
Evapotranspiration
Artificial wetland
Wetland-BGC

ABSTRACT

Wetlands play an important role in the exchange of carbon and energy between the land and the atmosphere. Moreover, wetlands are sensitive to global changes because of their unique water-heat effects and greenhouse gas (GHG) metabolic processes. However, the temporal variations in carbon and energy fluxes in wetlands are not yet fully understood. As an artificial wetland in an arid area, the Zhangye wetland features complex meteorological conditions and human interventions, which have introduced uncertainties into the carbon and energy fluxes. In this study, eddy covariance technology was used to examine the characteristics of the carbon and energy fluxes over an artificial wetland in an arid area. The main objectives were to determine (1) the diurnal and seasonal variations in the carbon and energy fluxes; (2) the relationship between the carbon and energy fluxes and the controlling factors, including the meteorological conditions and human interventions; (3) the contribution of carbon emissions from the wetland ecosystem; (4) the evapotranspiration (ET) difference between an artificial wetland in an arid region and a natural wetland; and (5) a preliminary simulation of net ecosystem exchange (*NEE*) and ET using the Biome-BGC model (Wetland-BGC version). Significant diurnal variations were observed in the carbon dioxide ($CO_2$) flux in different seasons, whereas variations in methane ($CH_4$) were not significant. Both $CO_2$ and $CH_4$ fluxes peaked in summer, with the highest emission rates occurring at 12:00–16:00 and featuring values of $-15.65\ \mu mol\ m^{-2}\ s^{-1}$ and $0.38\ \mu mol\ m^{-2}\ s^{-1}$, respectively. The $CO_2$ and $CH_4$ fluxes exhibited a strong relationship with soil temperature ($R^2 = 0.7305$ and 0.5949, respectively, for a soil depth of 0 cm). $CH_4$ emissions significantly influenced the total carbon budget, and the wetland was found to be a carbon sink with respect to the net exchange of carbon. The greatest ET in the Zhangye wetland during the study period was 12.33 mm $day^{-1}$, and the average annual ET was 1300.4 mm $year^{-1}$. This study examined the main components of the energy flux, including variations in the net radiation ($R_n$), latent heat flux (*LE*), sensible heat flux (*H*) and soil heat flux ($G_s$), and the relationships between these variables and the environmental controls. The range of $LE/R_n$ was 0.32–0.74, and this ratio was 0.64 during the growing season. The ratio of $H/LE$ ranged from −0.04 to 1.28, and the value was negative during June, July and August. Artificial wetlands had a large thermal capacity that tended to slow down the energy exchange. Human interventions, e.g., irrigation, policies, etc., significantly affected the $CH_4$ flux and ET but did not affect the $CO_2$ flux.



## 1. Introduction

Terrestrial ecosystems influence climate change through complex bio-geophysical feedback mechanisms, including the exchanges of carbon, water, and energy with the atmosphere (Beer et al., 2010; Bonan, 2008; Cao and Woodward, 1998; Heimann and Reichstein, 2008). Carbon dioxide ($CO_2$) and methane ($CH_4$) are the most important greenhouse gases (GHG), accounting for 70% and 23% of the rise in temperatures, respectively (Hendriks et al., 2007; Nnoby, 1997). The human activity has caused the volume fraction of $CO_2$ and $CH_4$ in the atmosphere to increase approximately 26% and 148%, respectively, after industrialization (Desai et al., 2015; Wang et al., 2010).

* Corresponding author.
*E-mail address:* sunrui@bnu.edu.cn (R. Sun).

http://dx.doi.org/10.1016/j.agrformet.2016.02.019

Wetlands are recognized as an important ecosystem and are estimated to store 15% of the total carbon in global terrestrial ecosystems (Kayranli et al., 2010; Liu and Zhou, 2012). Natural wetland ecosystems are widely considered to be a sink of free carbon from the atmosphere through high rates of net primary production and accumulation of organic matter in water-logged soils (Chen et al., 2013; Sun et al., 2009). However, the effects of artificial wetlands on the carbon budget are not well understood.

A typical Heihe Watershed wetland (the Zhangye wetland) is located in the middle of the Hexi Corridor, an extraordinarily complex ecosystem that contains rivers, marshes, wet meadows and artificial features. The Zhangye wetland is an artificial oasis in an arid region in northwestern China. The wetland's important roles, such as water purification, desertification control and climate adjustment, are in many ways based on its special geographical position. Flux measurements of the water, carbon and energy cycle here could contribute to an in-depth analysis of wetland ecosystems in arid areas.

$CO_2$ flux is the key to understanding the wetlands carbon cycle, which plays an important role in the carbon cycle of the continental ecosystem. Wetlands are also a primary natural source of $CH_4$ in the atmosphere (Chen et al., 2013). Energy exchange is among the most important processes in wetland ecosystems because it affects variables such as temperature, water transport, plant growth and productivity (Dennison and Berry, 1989). The main components of the surface energy balance are net radiation ($R_n$), the heat stored in water and soil, the sensible heat flux ($H$), and the latent heat flux ($LE$) or evapotranspiration (ET). ET in vegetated wetlands is frequently the largest consumer of incoming energy (Priban and Ondok, 1985) and greatly influences not only the energy distribution but also the water conditions, such as temperature and depth (Shukla and Mintz, 1982; Xiao et al., 2013).

At present, most of what is known regarding wetland ecosystem carbon and energy balances is confined to the temperate, boreal, and arctic zones, with data principally collected only during the growing season. Little is known about carbon and energy exchange in artificial wetlands, especially in arid regions where the climate conditions are complex and unique (Schedlbauer et al., 2011). The main objectives of this study were to determine (1) the diurnal and seasonal variations in carbon and energy fluxes; (2) the relationship between the carbon and energy fluxes and the controlling factors, including the meteorological conditions and human interventions; (3) the contribution of carbon emissions from the wetland ecosystem; (4) the difference in energy flux between an artificial wetland in an arid region and a natural wetland; and (5) a preliminary simulation of net ecosystem exchange (*NEE*) and ET using the Biome-BGC model.

## 2. Materials and methods

### 2.1. Basic information on the study area

The experimental area in this study, established in June 2012, is located in the midstream of the Heihe watershed, northwestern China. A flux tower was operated in the west of Zhangye National Wetland Park (100.44640°E, 38.97514°N) by the Heihe Watershed Allied Telemetry Experiment Research-the Multi-Scale Observation Experiment on Evapotranspiration over heterogeneous land surfaces (HiWATER-MUSOEXE) (Liu et al., 2011, 2013) (Fig. 1(A)).

The total area of the wetland park is 41.08 km$^2$, and the area of the actual wetland is 17.33 km$^2$. The primary vegetation in the study area is reeds, predominantly *Phragmites australis* with a mean height of 2.5–3.0 m. This plant leafs out in late April and is reaped at the end of October. The site has a warm, temperate continental climate, with 129 mm of annual precipitation, 2047 mm of average annual evaporation, a mean annual temperature of 6 °C and a mean annual frost-free period of 153 days.

The growing season of the study site is between May and October, during which more than 80% of the annual precipitation falls. July and January feature the highest and lowest mean temperatures, respectively.

### 2.2. Field measurements

#### 2.2.1. Eddy covariance measurements

$CO_2$, $CH_4$, $LE$ and $H$ fluxes were measured using the eddy covariance (EC) technique starting in July 2012. Open-path flux instruments were mounted on top of a mast with a sensor head 5.2 m above the wetland ecosystem (Fig. 1(B)).

Wind speed, wind direction and sonic temperature were measured using a three-dimensional ultrasonic anemometer (Gill, UK). An open-path fast-response infrared gas analyzer (Li-7500A, Li-Cor Inc., USA) was used to measure changes in $CO_2$ and $H_2O$ concentrations. The three-dimensional ultrasonic anemometer was located at a horizontal distance of 25 cm from the Li-7500A in the direction of the prevailing winds (north). The raw sampling frequency was 10 Hz, and mean fluxes for $LE$, $H$ and $CO_2$ were computed at 30-min intervals. Raw data and 30-min average data were recorded by a logger (CR1000, Campbell Scientific Instruments Inc., USA) every 30 min. $CH_4$ concentrations were measured using the open-path laser instrument LI7700 (Li-Cor Inc., USA). ET was measured directly using an energy-budget variant of the eddy correlation approach (Tanner and Greene, 1989; Twine et al., 2000).

#### 2.2.2. Meteorological measurements

Air temperature ($T_a$) and relative humidity (RH) were measured by HMP45C (Vaisala Inc., Helsinki, Finland). Air pressure (Pa) was measured by CS100 (Campbell Scientific Instruments Inc., USA); and precipitation (PPT) was measured with a tipping-bucket-type rain gauge placed above the canopy (TR-525M, Campbell Scientific Instruments Inc., USA).

Soil temperature ($T_s$, 107-L, Campbell Scientific Instruments Inc., USA) was measured at six depths (0.00, 0.02, 0.04, 0.10, 0.20 and 0.40 m). Ground heat ($G_s$) flux was also measured at this site using HFP01 (Avalon, Hukseflux, Netherland) heat flux transducers. Three soil heat plates were placed 5 cm below the soil surface. Incoming and outgoing photosynthetically active radiation (PAR) was measured using LI-190SA sensors (Li-Cor, Inc., USA). $R_n$ was measured with a four-component net radiometer (NR01, Avalon, Hukseflux, Netherland) at a height of 6 m.

### 2.3. Data analysis

All data were collected over a period of two years (July 2012–June 2014). EC flux data can be significantly affected by weather conditions, human disturbances and the limitations of the instruments (Saito et al., 2005). In this study, the energy balance was also analyzed, which was considered an independent part of the EC measurements (Li et al., 2005; Coulter et al., 2006).

#### 2.3.1. Quality control

The carbon and energy fluxes were calculated using the data-processing package EddyPro, version 4.1 (www.licor.com/eddypro), as described in the instrument manual and by McDermitt et al. (2011). The raw 10 Hz data were processed into the 30-min mean values, including spike detection, lag correction of $H_2O/CO_2$ and $CH_4$ relative to the vertical wind component, sonic virtual temperature correction, coordinate rotation (2-D rotation), density fluctuation corrections (Webb-Pearman-Leuning correction), and frequency response correction (Xu et al., 2013). Due to the significant effects associated with atmospheric stability, weather

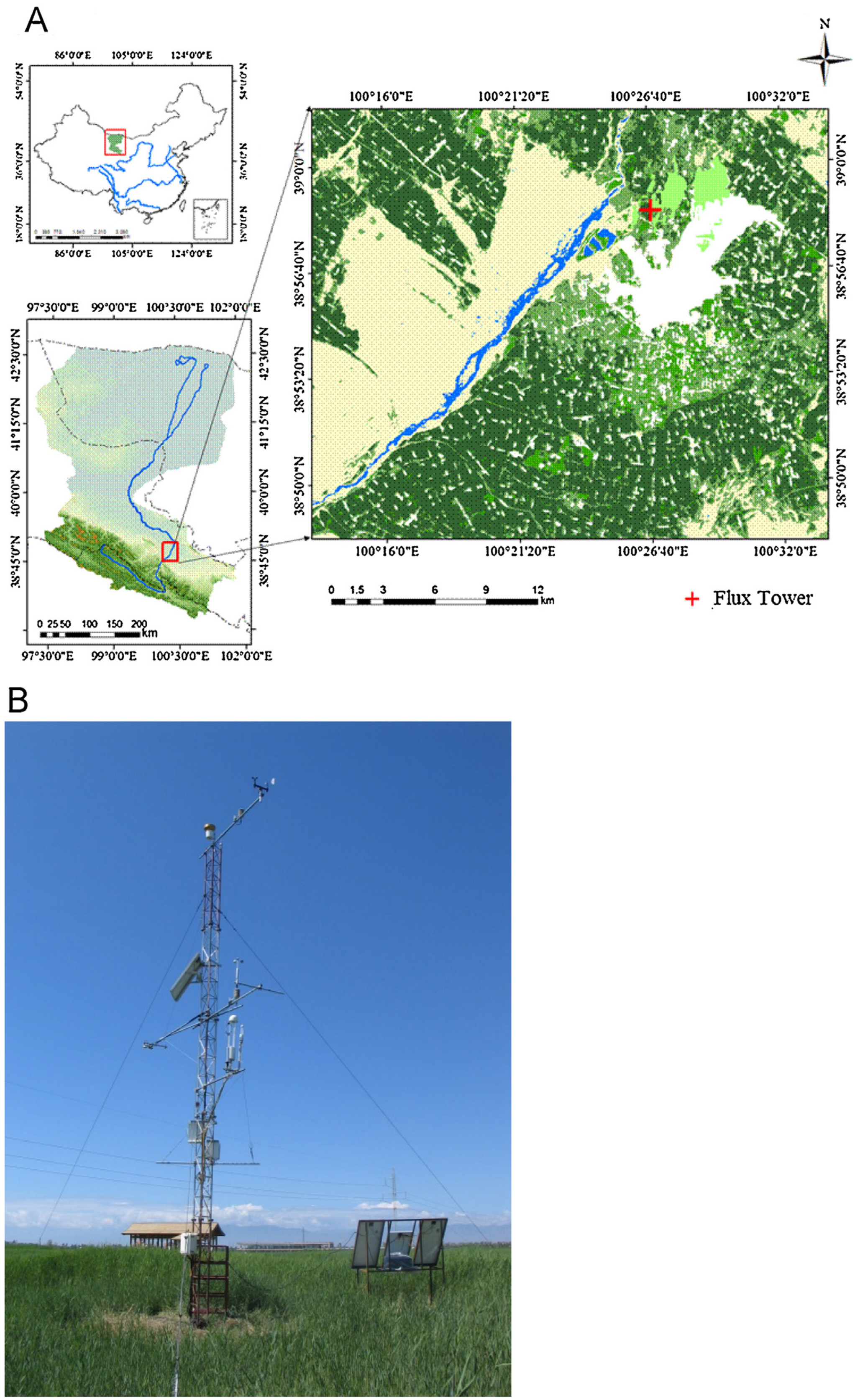


**Fig. 1.** Location map of the Zhangye wetland with the study site indicated (A) and the image of the eddy covariance tower (B).

conditions and the limitations of the instruments (Massman and Lee, 2002; Saito et al., 2005), the half-hour data were rejected if the data meet one or more of the following criteria (Aires et al., 2008): (1) rain events (one hour before or after the rain) (Falge et al., 2001), (2) nights when the $CO_2$ flux was negative (Papale et al., 2006; Zhu et al., 2006) (3) data beyond a reasonable range of the instrument

Please cite this article in press as: Zhang, Q., et al., Carbon and energy flux from a *Phragmites australis* wetland in Zhangye oasis-desert area, China. Agric. Forest Meteorol. (2016), http://dx.doi.org/10.1016/j.agrformet.2016.02.019

measurement (Papale et al., 2006; Zhu et al., 2006), and/or (4) cases when the value of $U^*$ was below the critical value (Papale et al., 2006; Zhu et al., 2006). Based on the mean-value test method (Zhu et al., 2006), the value of $U^*$ was set to 0.12 m $s^{-1}$ in this study.

#### 2.3.2. Gap-filling and data processing

Complete data sets were created using gap-filling. Missing time periods in the flux data were filled as follows: Gaps of less than 2 h were filled by linear interpolation between the nearest measured data points, whereas long-term gaps were filled using the look-up Table (LUT) method as described by Falge et al. (2001).

For the remaining missing periods, gap-filling was performed for the half-hourly fluxes. For the $CH_4$ flux, the half-hourly $CH_4$ flux data were first gap-filled using the same exponential relationship between $CH_4$ emissions and air temperature that was used for the daily approach. Then, a simple look-up Table was applied. The LUT parameters were $T_a$, PAR and PPT, and the LUT window size was initially set to 7 days. In the few cases where an LUT estimate was still not possible, gaps were filled by linear interpolation (Hommeltenberg et al., 2014). The LUT method was also used to gap-fill the energy flux data set.

Gross primary production (*GPP*) was calculated from ecosystem respiration ($R_{eco}$) and *NEE* (Zhang et al., 2015):

$$GPP = R_{eco} - NEE$$

*GPP* (mg $CO_2$ $m^{-2}$ $s^{-1}$) represents $CO_2$ assimilated by photosynthesis, and $R_{eco}$ (mg $CO_2$ $m^{-2}$ $s^{-1}$) represents respiratory $CO_2$ released from the soil and vegetation. Nighttime *NEE* values were equal to $R_{eco}$ because the *GPP* equals zero at night. Daytime $R_{eco}$ values were estimated using the nighttime *NEE*-temperature relationship. The relationship between nighttime *NEE* and $T_a$ can be described by the Vant Hoff equation (Lloyd and Taylor, 1994):

$$R_{eco} = ae^{bT_a}$$

where $a$ and $b$ were regression parameters and $T_a$ was the air temperature. Missing nighttime data were estimated using an exponential regression, based on the measured nighttime $R_{eco}$ and $T_a$.

### 2.4. Biome-BGC model

The Biome-BGC model, a process-based terrestrial ecosystem carbon cycle model, can estimate three vital biogeochemical cycles: carbon, nitrogen and water (Running and Hunt, 1993 Thornton, 1998). The version of the Wetland-BGC model we used in this study features an improvement in the simulation of the water state. This improvement better approximates the real conditions of plant growth in the wetland. The changes in water depth were calculated based on different conditions separately. In addition, infiltration was considered in the Wetland-BGC model, thereby potentially modifying the soil environment and influencing soil decomposition.

The ET in the BIOME-BGC (Wetland-BGC version) is estimated using the Penman-Monteith equation. Energy available in the canopy is divided into two parts: evaporation of water intercepted by the canopy and transpiration. The Farquhar photosynthesis routine (Farquhar et al., 1980) is used to calculate the biome *GPP*. Respiration components (heterotrophic ($R_h$), autotrophic growth ($R_g$) and autotrophic maintenance ($R_m$)) were calculated primarily based on temperature. *NEE* is defined as the *GPP* minus the respiration and defoliation rates ($D_r$):

$$NEE = GPP - R_h - R_g - R_m - D_r$$

Detailed descriptions of this equation's logic were given by Running and Hunt (1993) and Thornton and Running (1999).The model inputs include three parts: (1) the meteorological data, including the maximum and minimum daily air temperatures ($T_{a\_max}$ and $T_{a\_min}$, °C), average temperatures ($T_{a\_ave}$, °C), PPT (cm), total diurnal mean solar radiation ($R_s$, W $m^{-2}$), and day length (DL, s); (2) location information, including the longitude, latitude, elevation, soil depth, soil particle composition, vegetation type, and the atmospheric $CO_2$ concentration changes; and (3) ecological parameters, including the specific leaf area (SLA), C:N ratio of leaves and fine roots, annual leaf and fine root turnover fraction, etc.

The outputs include *GPP* (kg C $m^{-2}$), net primary production (*NPP*, kg C $m^{-2}$), *NEE* (kg C $m^{-2}$), $R_m$ (kg C $m^{-2}$), $R_g$ (kg C $m^{-2}$) and $R_h$ (kg C $m^{-2}$), etc. ET was also estimated in the model.

## 3. Result

### 3.1. Meteorological conditions and leaf area index

The study area was characterized by strong seasonal variation in air temperature and precipitation, with the warmest temperature of 26.2 °C in July and the coldest value of −8.4 °C in January (Fig. 2(A)). The leaf area index (LAI) data were collected from 8-day MODIS production (MOD15A2, https://ladsweb.nascom.nasa.gov/data/search.html) during the study period. In all years leaf area index (LAI) changed rapidly during the growing season (Fig. 2(B)). The highest LAI (2.1) was in 2012.

### 3.2. Carbon flux

#### 3.2.1. Diurnal variation

The diurnal trends in the $CO_2$ and $CH_4$ fluxes for different periods, based on the data after gap-filling, are shown in Fig. 3. We examined 10 days in each period related to general stages of plant phenology: period 1 was the beginning of growing season (April 11th–20th), period 2 was the peak of the growing season (July 11th–20th), period 3 was the late growing season (September 11th–20th), and period 4 was the non-growing season (January 11th–20th). Average data were calculated for each period from July 2012 to June 2014.

As seen in Fig. 3(B), the diurnal $CO_2$ flux exhibits a single-valley-peak pattern. The $CO_2$ flux was less than 0 after sunrise because the photosynthesis of the reeds is stronger than the sum of autotrophic respiration and soil heterotrophic respiration. The peak value of $CO_2$ flux, −15.65 μ mol $m^{-2}$ $s^{-1}$, was at noon in period 2, which featured the same radiation trend. The $CO_2$ flux then trended from sink into source when photosynthesis stopped at night. At night, the $CO_2$ flux was greater than 0.

The diurnal $CH_4$ flux exhibited greater variability during the growing season than the $CO_2$ flux, which was similar across the different periods. Fig. 3(A) shows the $CH_4$ diurnal variations in each period. The magnitude of the $CH_4$ flux was smaller than $CO_2$ and was in the range of 0–0.20 μ mol $m^{-2}$ $s^{-1}$. $CH_4$ emission in daytime was higher than nighttime during all the periods and the peak value of $CH_4$ flux occurred at approximately noon.

The highest $CH_4$ flux was in period 2, with a range of 0.1–0.4 μ mol $m^{-2}$ $s^{-1}$ during the peak growing season. In contrast, period 4 featured the lowest values, approximately 0.01 μ mol $m^{-2}$ $s^{-1}$.

#### 3.2.2. Seasonal variations

The average monthly $CO_2$ and $CH_4$ flux during study period is shown in Fig. 4. The ranges of $CO_2$ and $CH_4$ fluxes differed among the different growing periods. As shown in Fig. 4(A), from November to February, $R_{eco}$ was between 37.07 to 54.41 g $CO_2$ $m^{-2}$ $month^{-1}$, whereas monthly *GPP* was 0. This period was the non-growing season in the study area. At the beginning of study area's growing season, i.e., March, April, and May, *GPP* was 78.30,

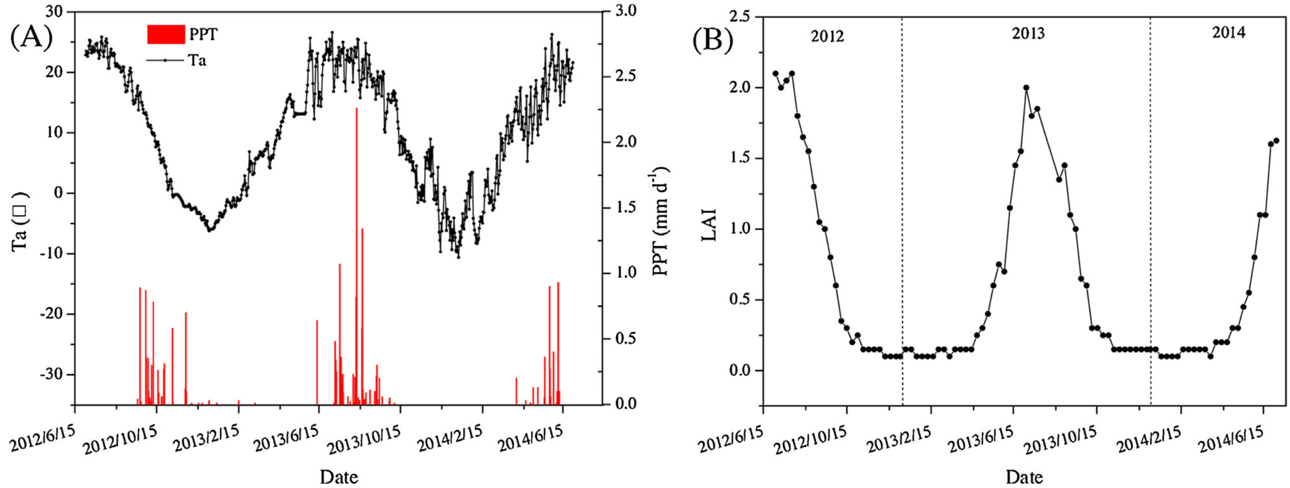


**Fig. 2.** Seasonal and interannual variation in (A) daily air temperature ($T_a$) and precipitation (PPT) and (B) daily leaf area index (LAI).

187.26 and 333.95 g $CO_2$ $m^{-2}$ $month^{-1}$, respectively. June–August was the peak period of the growing season with the highest $R_{eco}$ and *GPP*. The range of *GPP* during this period was 757.84–925.84 g $CO_2$ $m^{-2}$ $month^{-1}$, and $R_{eco}$ was between 421.19 and 440.17 g $CO_2$ $m^{-2}$ $month^{-1}$. *GPP* began to decrease after September: *GPP* in September and October was 459.16 and 155.38 g $CO_2$ $m^{-2}$ $month^{-1}$, respectively.

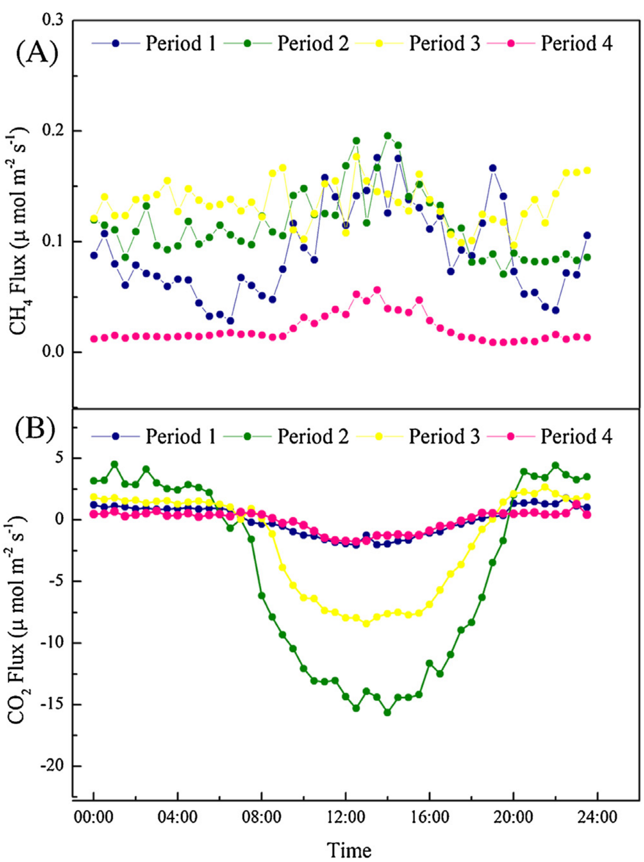


**Fig. 3.** The average daily variations in carbon flux based on the average value in different growth stages of the reeds. Period 1 was the beginning of growing season (April 11th–20th), period 2 was the peak of the growing season (July 11th–20th), period 3 was the late growing season (September 11th–20th), and period 4 was the non-growing season (January 11th–20th). (A) $CH_4$ flux ($\mu$ mol $m^{-2}$ $s^{-1}$), (B) $CO_2$ flux ($\mu$ mol $m^{-2}$ $s^{-1}$).

Fig. 4(B) shows that the $CH_4$ flux in the non-growing season was the lowest, amounting to 0.55–1.35 g C $m^{-2}$ $month^{-1}$. The $CH_4$ flux increased rapidly in March and April, reaching 1.80 and 2.65 g C $m^{-2}$ $month^{-1}$, respectively. The $CH_4$ flux between June and

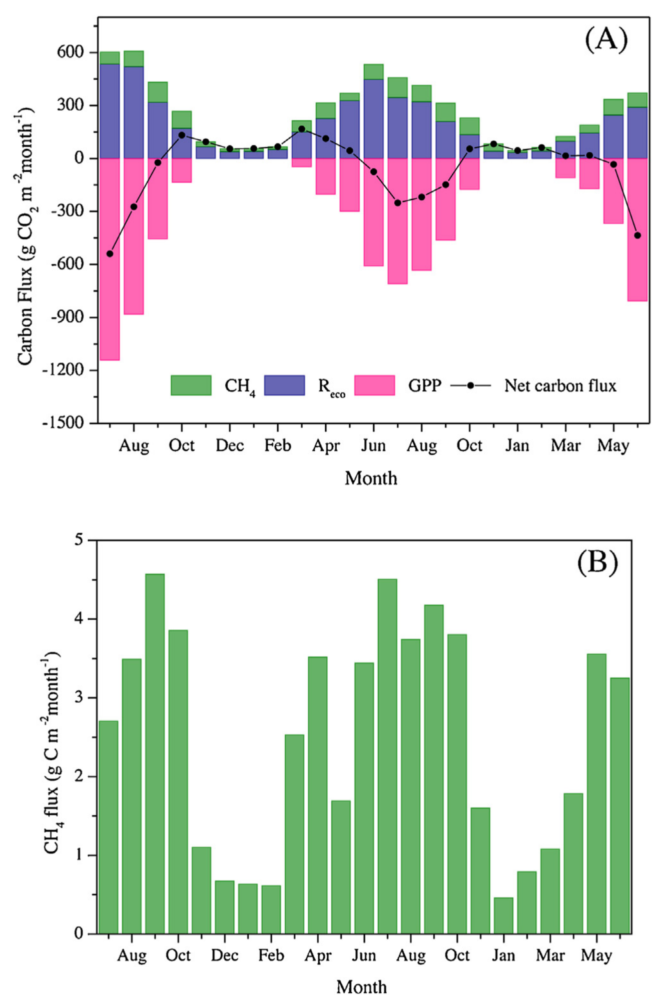


**Fig. 4.** Carbon flux in the study site during the study period with (A) carbon flux and (B) $CH_4$ flux. To compare the carbon source and sink more intuitively, opposite numbers of *GPP* were used in the figure.

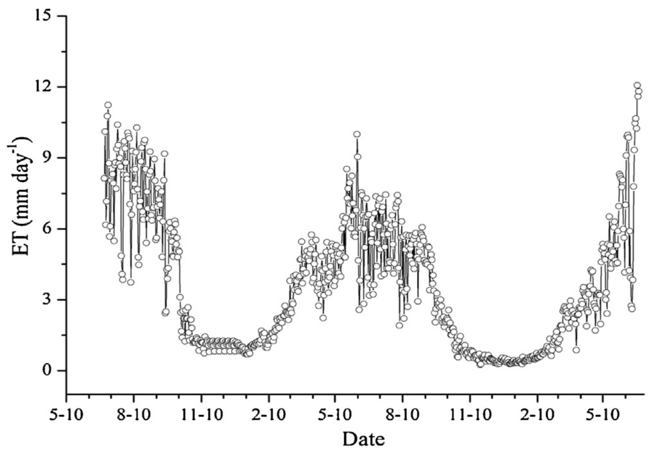


**Fig. 5.** Seasonal and annual variations in daily ET (mm day$^{-1}$) in the study area from July 2012 to June 2014.

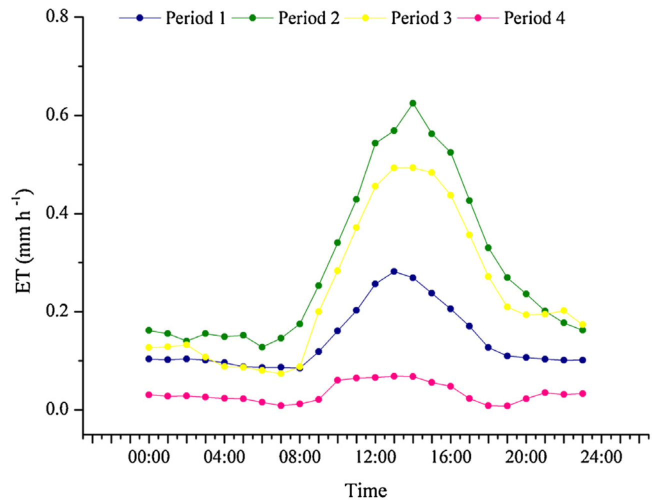


**Fig. 6.** Diurnal ET (mm h$^{-1}$) in different periods.

October was 18.77 g C m$^{-2}$ month$^{-1}$, representing 65.66% of the total $CH_4$ emissions observed during the study period.

The magnitude of the $CH_4$ flux was lower than the $CO_2$ flux, but the contribution of methane emissions to the global warming potential (GWP) on the 100-year time horizon can be expressed as the $CO_2$ equivalent (Hendriks et al., 2007; Hommeltenberg et al., 2014). The $CH_4$ GWP is 25 times stronger than that of $CO_2$ (IPCC Climate Change, 2007; Long et al., 2010; Hommeltenberg et al., 2014). The final carbon flux result for the study period represents the carbon pool (−44.57 g $CO_2$ m$^{-2}$ year$^{-1}$) with the $CH_4$ emissions converted using the GWP.

*3.2.3. Annual flux*

The annual *GPP* was 1.03 kg C m$^{-2}$ year$^{-1}$ from July 2012 to June 2013 and 0.94 kg C m$^{-2}$ year$^{-1}$ from July 2013 to June 2014. The average *GPP* during the research period was 0.98 kg C m$^{-2}$ year$^{-1}$. The annual *NEE* was −0.31 kg C m$^{-2}$ year$^{-1}$ and −0.47 kg C m$^{-2}$ year$^{-1}$ in the two research years, respectively.

The annual $CH_4$ flux was 27.76 g C m$^{-2}$ year$^{-1}$ from July 2012 to June 2013 and 28.75 g C m$^{-2}$ year$^{-1}$ from July 2013 to June 2014. The average $CH_4$ flux during the research period was 28.25 g C m$^{-2}$ year$^{-1}$, which was higher than the results of previous studies (Wille et al., 2008; Jackowicz-Korczynski et al., 2010; Hanis et al., 2013).

*3.3. ET*

The maximum rates of ET were recorded in the growing season, whereas the lowest rate (approximately zero) occurred in winter (Fig. 5). The highest ET (12.33 mm day$^{-1}$) occurred in June 2014, and the peak values in 2012 and 2013 were 11.24 mm day$^{-1}$ and 10.00 mm day$^{-1}$, respectively. The average ET was 5.21 mm day$^{-1}$ during the growing season and 1.22 mm day$^{-1}$ during the non-growing season. In winter, the average ET was 0.50 mm day$^{-1}$, and most of the records were <1.0 mm day$^{-1}$. The annual ET was 1507.9 mm year$^{-1}$ between July 2012 and June 2013 and 1092.8 mm year$^{-1}$ between July 2013 and June 2014.

Fig. 6 is the diurnal variation in ET for different periods. ET increased at 8:00 and decreased at 20:00, with a peak between 12:00 and 16:00. ET was the highest in period 2, reaching 0.62 mm h$^{-1}$. In period 1, the peak ET was 0.28 mm h$^{-1}$ at noon and was related to the beginning of snow melting and reed growing. In period 3, due to lower precipitation than the peak growing season and the cessation of plant growth, ET decreased significantly, with the highest rate of 0.49 mm h$^{-1}$ occurring at 12:30.

*3.4. Energy flux*

*3.4.1. Diurnal variation*

The diurnal energy flux for different periods of plant growth was calculated using the same period of carbon flux. The diurnal variation in energy flux (both *LE* and *H*) changed with $R_n$. In the non-growing season, $R_n$ reached as high as 264 W m$^{-2}$, and *LE* and *H* peaked at 127 W m$^{-2}$ and 47 W m$^{-2}$, respectively. In the peak growing season and post-peak growing season, the highest values of $R_n$ increased to 620 W m$^{-2}$ at noon in July, and *LE* increased dramatically to 428 W m$^{-2}$ in July, whereas *H* only reached 80 W m$^{-2}$ as the maximum value in September. *H* was highest at the beginning of the growing season, with a range of 34–201 W m$^{-2}$. The nighttime *LE* ranged from −30 to 30 W m$^{-2}$. The negative *LE* flux may be related to the heavy dew often observed at night. *LE* was the prime sink of $R_n$ in the wetland ecosystem (Fig. 7). Both *LE* and *H* peaked one to two hours after $R_n$ peaked (Fig. 7). This pattern was likely due to enhanced ET in the afternoon due to higher air temperature and vapor pressure deficit (VPD).

*3.4.2. Seasonal variation*

Fig. 8 shows the seasonal variations in energy flux in 2013 for the study area. $R_n$ increased during the growing season, with the highest air temperature and precipitation for the whole year, and declined during the non-growing season. The effects of environmental factors on $R_n$ varied among the seasons based on the influences on *LE* and *H*. During May to September, the $R_n$ was mainly used in ET, whereas *H* dominated in the cool months. The average $R_n$ was 280.24 W m$^{-2}$ during the growing season and 130.81 W m$^{-2}$ during the non-growing season. *LE* had a similar trend as $R_n$, reaching 172.71 W m$^{-2}$ during the growing season and 40.61 W m$^{-2}$ during the remaining period. The *LE* values were higher than *H* from March to October in the study area. Additionally, the trend of *H* from May to September was the opposite of the *LE* trend. The average *H* during the growing and non-growing seasons was 2.47 W m$^{-2}$ and 27.54 W m$^{-2}$, respectively.

*3.4.3. Energy ratio*

The partitioning of $R_n$ into *LE* and *H* affects the transport of the heat and water vapor in the atmosphere, which influences the ET of the study area, as well as regional and global precipitation (Dirmeyer, 1994; Pielke, 2001). The proportion for the allocation of $R_n$ into *LE* (*LE*/$R_n$) and *H* (*H*/$R_n$) varied significantly over time (Fig. 9). During the growing season, *LE*/$R_n$ and *H*/$R_n$ varied inversely: *LE*/$R_n$ dominated over *H*/$R_n$ from March to October, and vice versa for

Please cite this article in press as: Zhang, Q., et al., Carbon and energy flux from a *Phragmites australis* wetland in Zhangye oasis-desert area, China. Agric. Forest Meteorol. (2016), http://dx.doi.org/10.1016/j.agrformet.2016.02.019

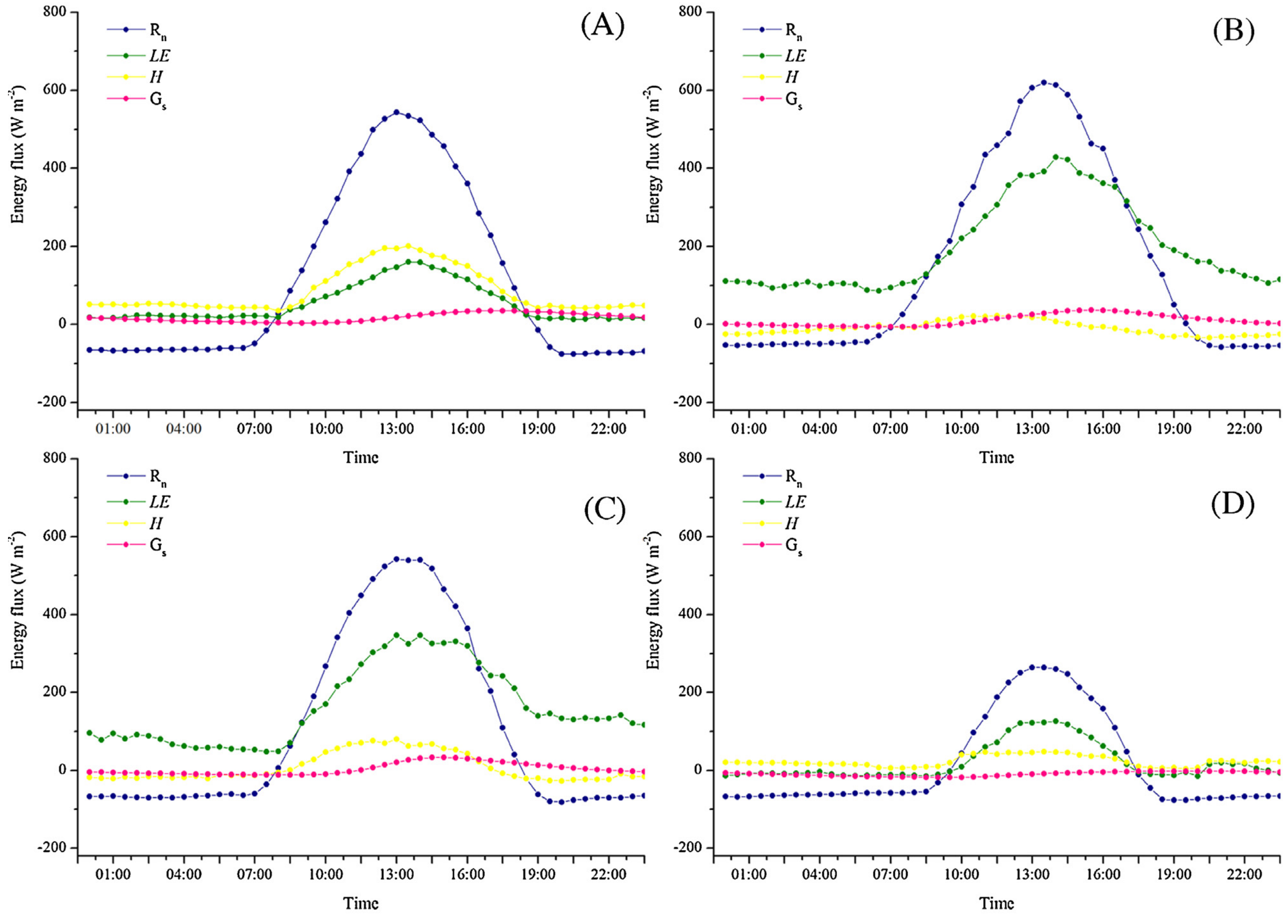


**Fig. 7.** Diurnal energy flux ($R_n$, *LE*, *H* and $G_s$) for each season in the study area. The periods are the same as for the carbon flux.

the remaining period. Approximately 45% to 74% of $R_n$ was partitioned into *LE* during the growing season, whereas 16% to 45% of $R_n$ was partitioned into *H* in the remaining period. On an annual basis, the portion of $R_n$ consumed in $G_s$ was low, accounting for approximately 3% in the study area. Water bodies containing low-temperature ice allowed $G_s/R_n$ to dominate in the winter months (December, January and February) when $G_s$ was predominant in the cold season. The absolute value of $G_s/R_n$ decreased during the growing season.

Fig. 10 shows the energy ratio of *H*/*LE* in 2013. The *H*/*LE* ratio had high values during the non-growing season, with a range of 0.42–1.28. However, this ratio was as low as −0.04 in July and August, which featured the highest ET rates of the whole year.

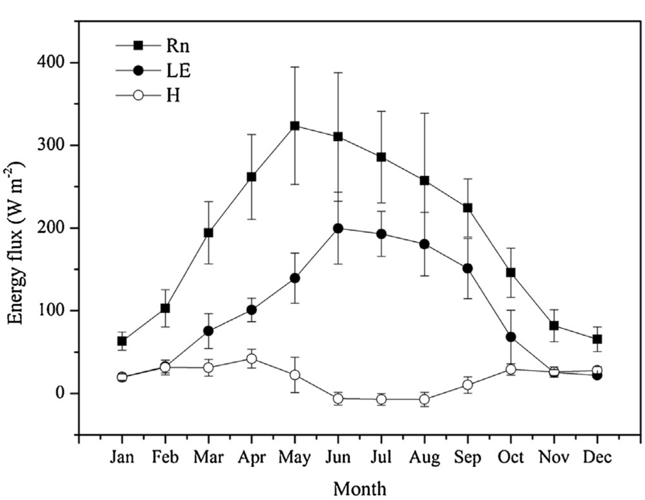


**Fig. 8.** Average monthly $R_n$, *LE* and *H* at the study site. Monthly energy flux from January to June is the mean of year 2013 and 2014, whereas the flux from July to December was calculated as the average of year 2012 and 2013.

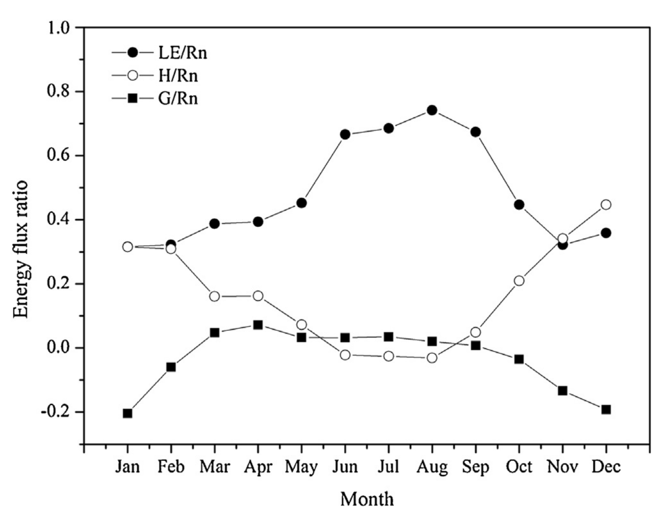


**Fig. 9.** Monthly energy ratios (*LE*/$R_n$, *H*/$R_n$ and $G_s/R_n$) during the study period. The method used to calculate the monthly average energy flux was as the same as Fig. 8.

Please cite this article in press as: Zhang, Q., et al., Carbon and energy flux from a *Phragmites australis* wetland in Zhangye oasis-desert area, China. Agric. Forest Meteorol. (2016), http://dx.doi.org/10.1016/j.agrformet.2016.02.019

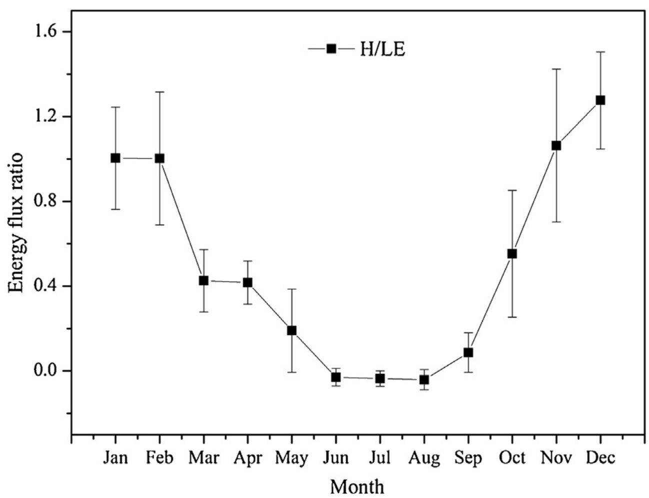


**Fig. 10.** Energy flux ratio (*H*/*LE*) calculated each month. The method used to calculate the monthly average energy flux was as the same as Fig. 8.

### 3.4.4. Energy balance closure

In this study, the energy balance closure was also examined based on the energy balance framework:

$$R_n - G_s = LE + H$$

Summed daily *LE* and *H* fluxes were plotted as a function of the daily $R_n - G_s$, as shown in Fig. 11. The sum of *LE* and *H* equals 66.34% of the available energy in 2013, 69.27% during the growing season and 59.77% during the non-growing season.

### 3.5. Model result

The Wetland-BGC version of the Biome-BGC model was used to simulate diurnal *NEE* and ET in the study area. A number of the parameters were modified before being used. Based on the environmental factors and the characteristics of the vegetation, we modified the phenology, C:N ratio and canopy light extinction coefficient to ensure they were more realistic.

Fig. 12 is a comparison between the modeled and observed *NEE* and ET values from July 2012 to June 2014. As shown in this figure, ET was overestimated during the growing season, but most of the overestimated values for *NEE* were in non-growing season. We used the root mean square error (RMSE) between the model simulation and the observation to evaluate the accuracy of the model simulation. The RMSE values for *NEE* and ET were 7.60 and 2.63, respectively. The coefficient of determination ($R^2$) values between the model simulation and flux observation for *NEE* and ET were 0.3065 and 0.6467, respectively.

The trends in the study site's production and ET can be modeled in the Biome-BGC model (Wetland-BGC version), but large errors and uncertainty exist in the model simulation. Model improvements will be researched further in the future.

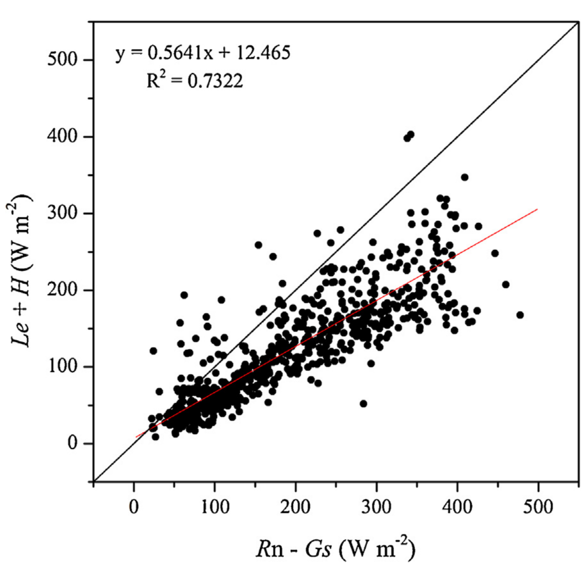


**Fig. 11.** Daily *H* and *LE* fluxes plotted as a function of the daily $R_n$ minus the $G_s$.

## 4. Discussion

### 4.1. A strong correlation between carbon and energy fluxes and environmental factors

#### 4.1.1. Temperature (air temperature and soil temperature)

*4.1.1.1. Carbon fluxes.* The diurnal $CO_2$ flux had a strong relationship of the air temperature and soil temperature. A linear fit was established between the diurnal $CO_2$ flux and the temperature (Table 1). The $R^2$ value between $CO_2$ and the shallow depths (0, 2 and 4 cm) was higher ($R^2 > 0.7$) than that of the deeper depths (10, 20 and 40 cm). Polynomial fitting was used to compare the correlation between $CO_2$ and deeper soil temperatures. The equations and $R^2$ values for each depth were different, but the $R^2$ values of the polynomial fit for the 10, 20 and 40 cm depths (0.7196, 0.6802 and 0.6377, respectively) were higher than those of the linear fits.

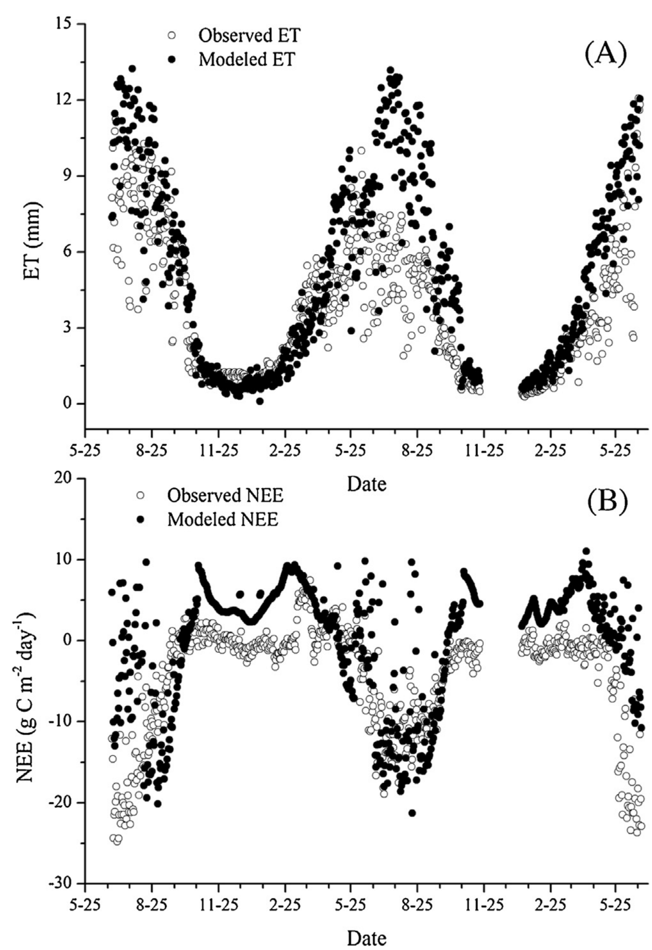


**Fig. 12.** Annual variations in the modeled and observed (A) ET (mm day $^{-1}$) and (B) *NEE* (g C m$^{-2}$ day$^{-1}$) for the study site from July 2012 to June 2014.

Please cite this article in press as: Zhang, Q., et al., Carbon and energy flux from a *Phragmites australis* wetland in Zhangye oasis-desert area, China. Agric. Forest Meteorol. (2016), http://dx.doi.org/10.1016/j.agrformet.2016.02.019

**Table 1**
Calculations of the values of coefficients (a and b) and the proportion of variance explained ($R^2$) by a linear fit (equation: y = ax + b) applied to the daily average $CO_2$ and $CH_4$ fluxes and different daily average temperatures (air temperature and soil temperature measured at 0, 2, 4, 10, 20 and 40 cm depths).

| | | $T_a$ | $T_{s\text{-}0\,cm}$ | $T_{s\text{-}2\,cm}$ | $T_{s\text{-}4\,cm}$ | $T_{s\text{-}10\,cm}$ | $T_{s\text{-}20\,cm}$ | $T_{s\text{-}40\,cm}$ |
|---|---|---|---|---|---|---|---|---|
| $CO_2$ | a | 0.4729 | 0.489 | 0.4916 | 0.4941 | 0.4985 | 0.507 | 0.5451 |
| | b | 2.0484 | 1.8995 | 1.9288 | 1.9817 | 2.1133 | 2.0233 | 1.9276 |
| | $R^2$ | 0.7205 | 0.7305 | 0.7095 | 0.7115 | 0.6821 | 0.6374 | 0.5795 |
| $CH_4$ | a | 0.0499 | 0.0478 | 0.0476 | 0.0481 | 0.0489 | 0.0481 | 0.0470 |
| | b | 0.0581 | 0.0622 | 0.0632 | 0.0632 | 0.0637 | 0.0654 | 0.0714 |
| | $R^2$ | 0.5440 | 0.5949 | 0.5897 | 0.5855 | 0.5604 | 0.5338 | 0.4998 |

**Table 2**
Calculations of the values of coefficients (a and b) and the proportion of variance explained ($R^{2f}$) by an exponential fit (equation: $y = a\,e^{bx}$) applied to the daily ET data and the various daily average temperatures (air temperature and soil temperature measured at 0, 2, 4, 10, 20 and 40 cm depths).

| | $T_a$ | $T_{s\text{-}0\,cm}$ | $T_{s\text{-}2\,cm}$ | $T_{s\text{-}4\,cm}$ | $T_{s\text{-}10\,cm}$ | $T_{s\text{-}20\,cm}$ | $T_{s\text{-}40\,cm}$ |
|---|---|---|---|---|---|---|---|
| a | 1.0766 | 1.1426 | 1.1474 | 1.1603 | 1.1949 | 1.1897 | 1.1810 |
| b | 0.0836 | 0.0807 | 0.0810 | 0.0812 | 0.0810 | 0.0810 | 0.0841 |
| $R^2$ | 0.7283 | 0.7197 | 0.6949 | 0.6939 | 0.6457 | 0.5804 | 0.5147 |

The diurnal $CH_4$ flux was strongly correlated with changes in the diurnal air and soil temperatures, a finding that had been reported by many other studies (Lai, 2009; Whalen, 2005). In this study, the measurements of soil temperature were restricted to 0, 2, 4, 10, 20 and 40 cm depths (Table 1). The 0 cm depth soil temperature exhibited the strongest correlation (linear fit) with the $CH_4$ flux, with an $R^2$ of 0.5949. The air temperature also played an important role in the relationship between $CH_4$ flux and temperature, with an $R^2$ of 0.5440.

In addition, snowmelt played an important role in $CH_4$ emission in late March and early April when $CH_4$ emissions increased rapidly in both 2013 and 2014 (Fig. 13). In contrast, the $CH_4$ flux during the non-growing season was close to 0 due to the ice. The emission of $CH_4$ requires the water table to be close to the surface: anoxic soil conditions suppress methanotrophic processes and enhance methanogenic processes. This principle had been confirmed by many studies that found increasing $CH_4$ emissions with rising water tables (Limpens et al., 2008). We were not able to consider the water table because a water-level gauge was not present. Thus, the relationship between the water table and $CH_4$ emissions is still unknown in this area. In addition to the studies mentioned above, many other studies have also identified the water table as an important factor in $CH_4$ emissions (Raddatz et al., 2009; Godwin et al., 2013; Nadeau et al., 2013).

*4.1.1.2. Energy fluxes.* A strong relationship existed between ET and temperature, including both air temperatures and soil temperatures (Jacobs et al., 2002). An exponential fit was used to explain the correlations (Table 2). The range of $R^2$ values was 0.5147 ($T_{s\text{-}40cm}$)–0.7283 ($T_a$), indicating that the correlation between air temperature and ET was strongest. In addition, when the soil depth was greater than or equal to 10 cm, a polynomial fit was more appropriate for evaluating the relationship (Fig. 13). The $R^2$ values increased 0.7%, 6.9% and 14.4% between ET and soil temperature for the depths of 10 cm, 20 cm and 40 cm, respectively.

### *4.1.2. PAR*

The relation between half-hour intervals PAR and ET, $CO_2$ and $CH_4$ fluxes were analyzed with Pearson's correlation analysis (Table 3). There was significant positive correlation ($P < 0.01$) between PAR and ET and the Pearson's correlation coefficient was 0.717–0.842 during the growing season. Half-hour intervals $CH_4$ flux over the growing season were weakly correlated with PAR than non-growing season (r = 0.597). Significant negative correlation was between PAR and $CO_2$ flux during both growing season and non-growing season.

**Table 3**
Pearson's correlation coefficients (r) between PAR and ET, $CO_2$ and $CH_4$.

| | Growing Season | | | Non-growing Season |
|---|---|---|---|---|
| | Period 1 | Period 2 | Period 3 | Period 4 |
| ET | 0.812** | 0.842** | 0.717** | 0.363** |
| $CO_2$ | −0.459** | −0.554** | −0.751** | −0.232** |
| $CH_4$ | 0.396** | 0.386** | 0.167** | 0.597** |

Significance of Pearson's correlation coefficients: **$P < 0.01$.

**Table 4**
Pearson's correlation coefficients (r) between $U^*$ and ET, $CO_2$ and $CH_4$.

| | Growing Season | | | Non-growing Season |
|---|---|---|---|---|
| | Period 1 | Period 2 | Period 3 | Period 4 |
| ET | 0.225** | 0.409** | 0.200** | 0.384** |
| $CO_2$ | −0.247** | −0.405** | −0.293** | −0.402** |
| $CH_4$ | 0.292** | 0.222** | 0.049 | 0.166** |

Significance of Pearson's correlation coefficients: **$P < 0.01$.

### *4.1.3. Others*

*4.1.3.1. $U^*$.* The half-hour variation in ET was significantly positive correlated (Pearson's correlation coefficient, r) with friction velocity ($U^*$), especially in period 2 (Table 4). The similar relation was between $U^*$ and $CO_2$ flux. But the correlation that occurred between $CH_4$ flux and $U^*$ was not statistically significant in period 3 ($P > 0.05$).

*4.1.3.2. VPD.* Diurnal variation in diurnal ET was strongly correlated with associated changes in diurnal VPD (Fig. 14). The fitted line was determined by non-linear, power function correlation, with $R^2 = 0.6465$.

*4.1.3.3. Phenology and water condition.* The variation in phenology was the main environmental factor associated with the seasonal variations in *LE* and *H*, which was similar to the findings of many previous studies (Admiral et al., 2006; Giambelluca et al., 2009; Goulden et al., 2007). However, phenology was not a unique factor in the study area because of the special environmental conditions, high latitude and dry air conditions surrounding the research area. The water body stored heat and had an important impact on heat exchange processes, making the heat exchange over the wetland stronger than that over dry-surface ecosystems (Lei and Yang, 2010; Li and Li, 2009). Thus, the water condition of a wetland in an arid region is one of the most important factors in the radiation allocations.

## *4.2. High ET of the artificial wetland in an arid area*

Due to the low precipitation (approximately 104.6 mm $year^{-1}$) and high ET (more than 1300.4 mm $year^{-1}$), the drought index of the study area was 12.43, indicating that this area was very dry. Surface water and groundwater were the most important sources of water for the wetland. Compared to natural wetlands, little was known about the artificial wetland. We collected several previous studies on ET in natural wetlands and other ecosystems with similar geographic situations as the Zhangye wetland ecosystem (Tables 5 and 6).

The annual ET in this study was similar to the average of the selected values observed in natural wetlands. However, the environment differs significantly between the Zhangye wetland and the natural wetlands. All of the wetland sites were located in humid areas with higher precipitation and lower ET than the Zhangye

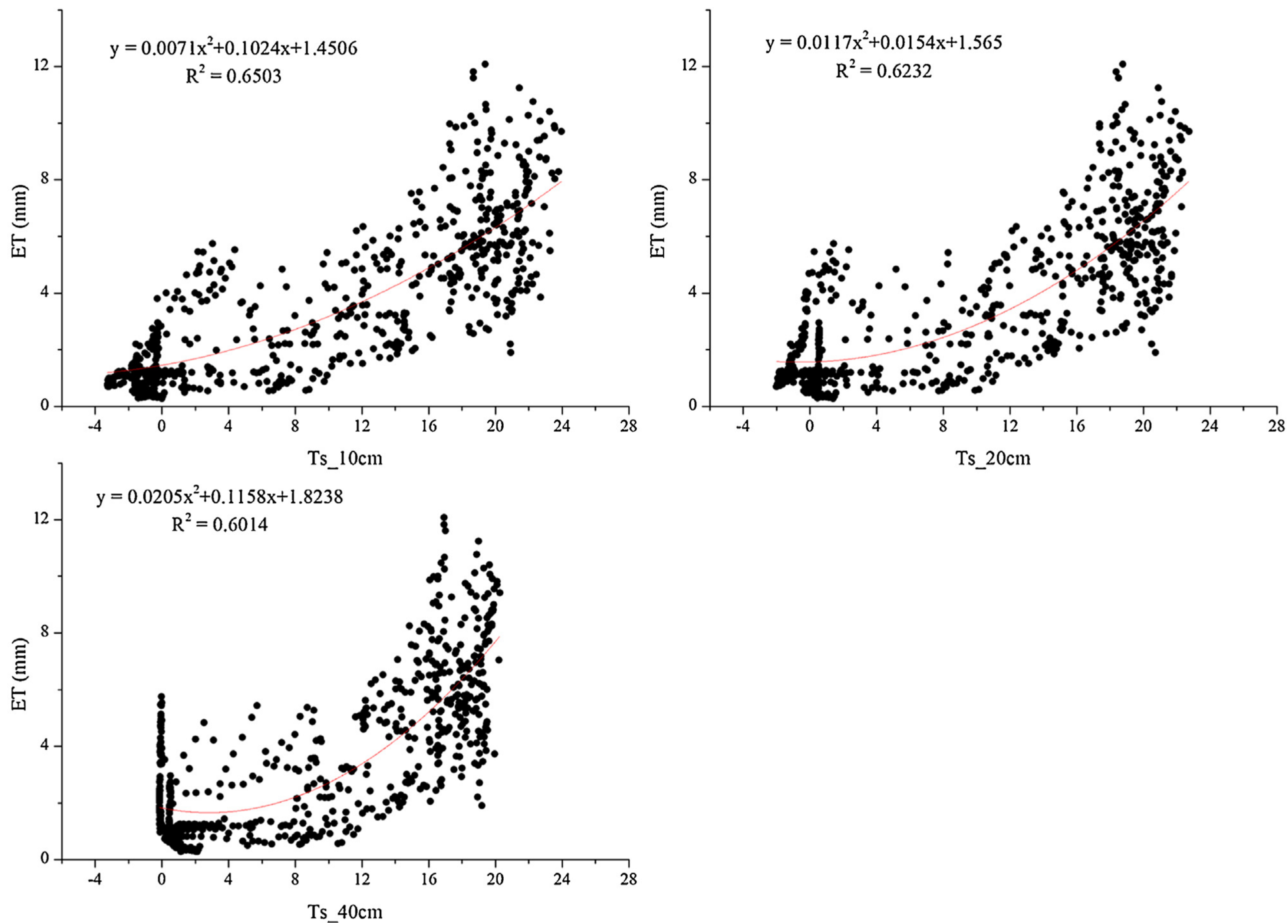


**Fig. 13.** Polynomial fit between diurnal ET and soil temperature (for the 10, 20 and 40 cm depths).

**Table 5**
Comparison of monthly ET in the Zhangye wetland and other natural wetlands.

| Study location (Latitude) | Wetland type | ET range (mean) mm $day^{-1}$ | References |
|---|---|---|---|
| Latitude between 30° and 40°N | | | |
| Freshwater marsh, California, 33°39′N | Bulrush-cattail marsh | 0.1–4 | Goulden et al. (2007) |
| Sicily, Italy 37°20′N | Reed dominated wetland | 0.8–8.0 | Borin et al. (2011) |
| Twitchell island, California 38°06′N | Cattail marsh (restored) | 0.8–12.2 (6) | Drexler et al. (2008) |
| Baiyangdian marsh, China 38°53′N | Reed dominated wetland | 10.7–20.9 (14.8) | Xu et al. (2011) |
| Latitude between 40° and 50°N | | | |
| Republican river basin, Nebraska 40°17′N | Reed and cattail dominated wetland | 0.1–8.2 (4.4) | Lenters et al. (2011) |
| Platte river basin, Nebraska, USA, 41°79′N | Riparian plant community | 0.3–11 (4.3) | Irmak et al. (2013) |
| China, 41°08′N | Marsh | 0.5–5.8 | Zhou and Zhou (2009) |
| USA, 42°30′N | Reed prairie wetland | 2.5–6.5 | Burba et al. (1999) |
| Veneto, Italy, 45°49′N | Reed dominated wetland | 0.7–5.0 | Borin et al. (2011) |
| KBW, Hungary, 46°47′N | Reed dominated wetland | 0.3–4.9 | Boldizsár (2007) |
| Zhalong, China, 46°52′N | Reed and cattail dominated wetland | 0.2–6.9 | Yao et al. (2010) |
| Sanjiang Plain China, 47°35′N | Sedge dominated marsh | 0.6–4.8 (2.3) | Sun and Song (2008) |
| Latitude >50°N | | | |
| James Bay Canada, 51°07′N | Coastal marsh, sedge | 2.6–3.1 | Lafleur (1990) |
| Kent, England, 51°19′N | Reed dominated wetland | 0.5–5.0 | Peacock and Hess (2004) |
| Himley, England, 52°31′N | Reed dominated wetland | 0.2–6.3 | Fermor et al. (2001) |
| Bornhoved lake, Germany, 54°06′N | Reed dominated wetland | 2.3–3.6 | Herbst and Kappen (1999) |
| Canada 56°04′N | Sub-humid western boreal plain wetland | 0.83–1.56 | Brown et al. (2010) |
| Canada, 58°40′N | Tundra sedge fen | 0.5–3.4 | Raddatz et al. (2009) |
| Northwestern Russia, 61°56′N | Boreal peatland fen | 0.45–5.6 (2.5) | Runkle et al. (2014) |

wetland. In contrast, surface water and groundwater was the most important source of water for Zhangye wetland.

Table 6 shows the ET from April to September 2013 for three other sites near the wetland site. All 4 sites shared similar locations (midstream of Heihe watershed) but different vegetation, including cropland, orchard and Gobi. The ET in the wetland was high in April and May, the beginning of growing season for the vegetation in the wetland, cropland and orchard. From June to August, ET in the cropland and orchard increased significantly due to regular irrigation, while ET in the wetland began to decrease. The Gobi

**Table 6**
Comparison of monthly ET in the Zhangye wetland and other sites with the same location (midstream of Heihe watershed) but with different vegetation, including cropland, orchard and Gobi (Ma, 2015).

| Types | Monthly ET (mm) | | | | | |
|---|---|---|---|---|---|---|
| | April | May | June | July | August | September |
| Wetland | 128.45 | 167.32 | 178.01 | 171.31 | 153.13 | 127.2 |
| Cropland | 63.14 | 102.1 | 141.78 | 151.1 | 127.96 | 93.99 |
| Orchard | 69.53 | 105.3 | 154.06 | 155.65 | 135.22 | 102.94 |
| Gobi | 33.75 | 57.19 | 50.52 | 35.98 | 29.05 | 26.82 |

had the lowest ET among the 4 sites due to sparse vegetation and little water.

### 4.3. Management significantly affects carbon and energy fluxes

The Zhangye wetland is an artificial wetland in an arid area. Human intervention is a major factor influencing the carbon and energy fluxes. This influence makes an artificial wetland different from a natural wetland. According to our survey, certain management practices occurred in the wetland during the study period.

#### 4.3.1. Irrigation

Abundant crops are present around the Zhangye wetland. During the crop growing season, regular irrigation was performed. The water level in the wetland decreased when the irrigation occurred.

#### 4.3.2. Policy

Zhangye should "share water" with another county (Mesozoic-Cenozoic, a county in the lower reaches of Heihe River). During the period of "sharing water", all irrigation was stopped, and the water level increased in the wetland. Three periods of "shared water", each 10–15 days long, occur during a year: June, July and September.

#### 4.3.3. Other human intervention

A channel around the flux tower was dug during December 2012–May 2013. This trenching leaded to a larger water area and less vegetation than in 2012. These effects might explain the decrease in ET and NEE between May 2012 and May 2013. However, in June to September 2013, the ET values were higher than in 2012 and 2014. These higher values may be due to changes in the quantity of water transported from the channel. The human interventions may have contributed to the variations in the carbon and energy fluxes. As shown in Fig. 15, the periods of increased $CH_4$ flux include late March and early April, mid-October, late June and early July and late September. The increase in late March and early April was related to physical cumulative emissions. $CH_4$ accumulated under the ice during the winter season and burst into the atmosphere in late March and early April in association with ice melt and higher air temperatures.

The high $CH_4$ emissions in mid-October were related to a lack of irrigation. When the crops were reaped, irrigation ceased, and the water level of wetland increased. In late June and early July and in late September, the water level increased because of the shared water policy. We could not quantify the channel's influences of the carbon and energy fluxes, but the $CH_4$ flux increased in May 2013 relative to the same period in 2014 in association with construction of the channel. The $CH_4$ stored in the soil may have been released when the channel was dug. The low-emissions periods were late July and early September. The decline in the $CH_4$ flux followed the drop in the water level associated with crop irrigation.

The variations in ET were similar to those of the $CH_4$ flux. Previous studies have found that the water table is the primary factor controlling $CH_4$ emissions (Godwin et al., 2013; Limpens et al., 2008; Nadeau et al., 2013; Raddatz et al., 2009) and ET (Long et al., 2010; Sun et al., 2011; Irmak et al., 2013).

In this study, the same relationship was observed between the water level and the $CH_4$ emissions and ET. This relationship differed from that of a natural wetland because the variations in water level in the studied wetland result from not only precipitation but also human interventions. In fact, human interventions primarily controlled the water level in the study area. No measurements of the water table were available for the wetland; thus, quantifying the relationship between water level and the carbon and energy fluxes is difficult.

The simulation based on the Biome-BGC model (Wetland-BGC version) overestimated the *NEE* and ET, possibly due to its failure to account for management practices. Vegetation and land cover can be changed by human intervention but these factors could be estimated by the model.

### 4.4. Is the artificial wetland in an arid area a carbon sink?

As described in Section 3.1, the $CH_4$ emissions were calculated using GWP to estimate the total greenhouse gas balance based on $CO_2$. The approach for the calculation of GWP was initially developed to determine the comparative impact of single-pulse emissions of both $CO_2$ and $CH_4$ to the atmosphere for a

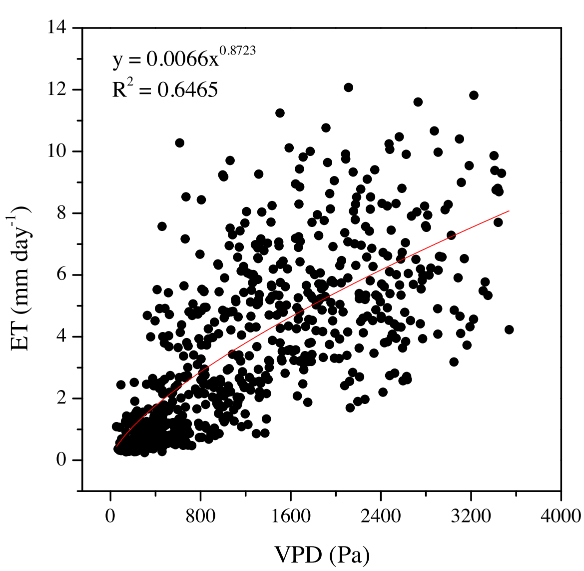


**Fig. 14.** Relationship between VPD (Pa) and diurnal ET (mm day$^{-1}$).

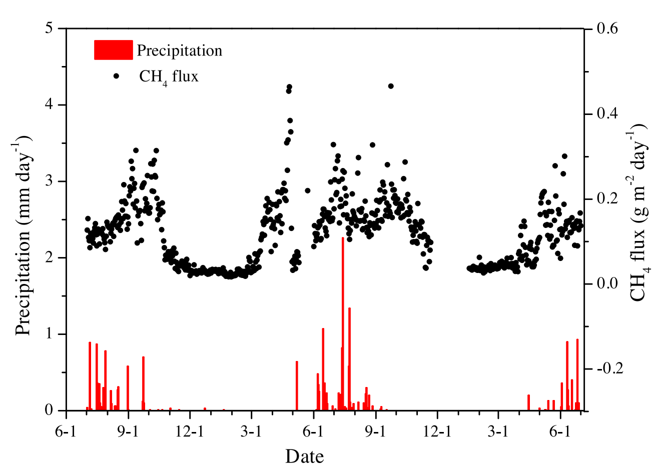


**Fig. 15.** Diurnal precipitation (mm day$^{-1}$) and $CH_4$ flux (g $CH_4$ m$^{-2}$ day$^{-1}$).

particular time period (Long et al., 2010). Our results indicate that the study site is more likely a greenhouse gas sink than a source. However, with the large uncertainty in the GWP balance, the application of the standard GWP calculation to the wetland ecosystem—atmosphere gas exchange is insufficient (Frolking et al., 2006). Thus, it could be concerned that Zhangye oasis-desert wetland was carbon sink during the study period. But we could not easily consider that it is a persistent carbon sink in this area.

## 5. Conclusions

We used the EC technique to determine the carbon and energy fluxes over an artificial wetland in an arid area. Both $CO_2$ and $CH_4$ fluxes exhibited strong relationships with temperature (air temperature and soil temperature) and PAR. During the study period, the wetland was a carbon sink based on the GWP calculations. The annual average ET between July 2012 and June 2014 was 1300.38 mm $year^{-1}$. The diurnal ET was primarily controlled by the variations in the soil temperatures, VPD and the latent heat flux. The simulated *NEE* and ET values based on the Biome-BGC model (Wetland-BGC version) featured similar trends as the observed values, but large uncertainties were present between the simulation and observations. The result of energy balance closure indicated that the sum of *LE* and *H* was equal to 66.34% of the available energy. Both the $CH_4$ flux and ET increased and decreased significantly during the study period. The water table was one of the most important factors influencing the $CH_4$ flux and ET. Compared with the environmental factors, human intervention was a more significant factor with respect to the GHG emissions in this artificial wetland than in natural wetlands.

## Acknowledgements

This work was supported by the National Natural Science Foundation of China (41471349, 91125002), the National Key Project of Scientific and Technical Supporting Programs Funded by Ministry of Science & Technology of China (2013BAC03B02), and the Fundamental Research Funds for the Central Universities (2014kJJCA02). The data used in the paper are from the Heihe Watershed Allied Telemetry Experimental Research experiment, we greatly thank all participants.

## References

Admiral, S.W., Lafleur, P.M., Roulet, N.T.L., 2006. Controls on latent heat flux and energy partitioning at a peat bog in eastern Canada. Agric. For. Meteorol. 140, 308–321.

Aires, L.M., Pio, C.A., Pereira, J.S., 2008. The effect of drought on energy and water vapour exchange above a Mediterranean C3/C4 grassland in Southern Portugal. Agric. For. Meteorol. 148 (4), 565–579.

Beer, C., Reichstein, M., Tomelleri, E., Ciais, P., Jung, M., Carvalhais, N., Rödenbeck, C., Arain, M.A., Baldocchi, D., Bonan, G.B., Bondeau, A., Cescatti, A., Lasslop, G., Lindroth, A., Lomas, M., Luyssaert, S., Margolis, H., Oleson, K.W., Roupsard, O., Veenendaal, E., Viovy, N., Williams, C., Woodward, F.I., Papale, D., 2010. Terrestrial gross carbon dioxide uptake: global distribution and covariation with climate. Science 329 (5993), 834–838.

Boldizsár, A., 2007. Examination of evaporation and microclimate in the reed canopies of Lake Balaton. In: Ph.D. Thesis. Univ. of Pannonia, Veszprém, Hungary.

Bonan, G.B., 2008. Forests and climate change: forcings, feedbacks, and the climate benefits of forests. Science 320 (5882), 1444–1449.

Borin, M., Milani, M., Salvato, M., Toscano, A., 2011. Evaluation of Phragmitesaustralis (Cav:) Trin. evapotranspiration in northern and southern Italy. Ecol. Eng. 37, 721–728.

Brown, S.M., Petrone, R.M., Mendoza, C., Devito, K.J., 2010. Surface vegetation controls on evapotranspiration from a sub-humid Western Boreal Plain wetland. Hydrol. Processes 24 (8), 1072–1085.

Burba, G.G., Verma, S.B., Kim, J., 1999. Surface energy fluxes of *Phragmites australisin* a prairie wetland. Agric. For. Meteorol. 94, 31–51.

Cao, M.K., Woodward, F.I., 1998. Net primary and ecosystem productions and carbon stocks of terrestrial ecosystems and their response to climate change. Global Change Biol. 4, 185–198.

Chen, Q.F., Ma, J.J., Liu, J.H., Zhao, C.S., Liu, W., 2013. Characteristics of greenhouse gas emission in the Yellow River Delta wetland. Int. Biodeterioration Biodegrad. 85, 646–651.

Coulter, R.L., Pekour, M.S., Cook, D.R., Klazure, G.E., Martin, T.J., Lucas, J.D., 2006. Surface energy and carbon dioxide fluxes above different vegetation types within ABLE. Agric. For. Meteorol. 136 (3–4), 147–158.

Dennison, M.S., Berry, J.F., 1989. Wetlands: Guide to Science, Law, and Technology. Noyes Publications, Park Ridge, pp. 439.

Desai, A.R., Xu, K., Tian, H.Q., Weishampel, P., Thom, J., Baumann, D., Andrews, A.E., Cook, B.D., King, J.Y., Kolka, R., 2015. Landscape-level terrestrial methane flux observed from a very tall tower. Agric. For. Meteorol. 201, 61–75.

Dirmeyer, P.A., 1994. Vegetation as a feedback mechanism in midlatitude drought. J. Clim. 7, 1463–1483.

Drexler, J.Z., Anderson, F.E., Snyder, R.L., 2008. Evapotranspiration rates and cropcoefficients for a restored marsh in the Sacramento-San Joaquin Delta, California, USA. Hydrol. Processes 22, 725–735.

Falge, E., Baldocchi, D., Olson, R., Anthoni, P., Aubinet, M., Bernhofer, C., Burba, G., Ceulemans, R., Clement, R., Dolman, H., Granier, A., Gross, P., Grünwald, T., Hollinger, D., Jensen, N.O., Katul, G., Keronen, P., Kowalski, A., TaLai, C., Law, B.E., Meyers, T., Moncrieff, J., Moors, E., WilliamMunger, J., Pilegaard, K., Rannik, Ü., Rebmann, C., Suyker, A., Tenhunen, J., Tu, K., Verma, S., Vesala, T., Wilson, K., Wofsy, S., 2001. Gap filling strategies for long term energy flux data sets. Agric. For. Meteorol. 107, 71–77.

Farquhar, G.D., von Caemmerer, S., Berry, J.A., 1980. A biochemical model of photosynthetic $CO_2$ assimilation in leaves of $C_3$ species. Planta 149, 78–90.

Fermor, P.M., Hedges, P.D., Gilbert, J.C., Gowing, D.J.G., 2001. Reed bed evapotranspiration rates in England. Hydrol. Processes 15, 621–631.

Frolking, S.E., Roulet, N., Fuglestvedt, J., 2006. How northern peatlands influence the Earth's radiative budget: sustained methane emission versus sustained carbon sequestration. J. Geophys. Res. Biogeosci. 111.

Giambelluca, T.W., Scholz, F.G., Bucci, S.J., Meinzer, F.C., Goldstein, G., Hoffmann, W.A., Franco, A.C., Buchert, M.P., 2009. Evapotranspiration and energy balance of Brazilians savannas with contrasting tree density. Agric. For. Meteorol. 149, 1365–1376.

Godwin, C.M., McNamara, P.J., Markfort, C.D., 2013. Evening methane emission pulses from a boreal wetland correspond to convective mixing in hollows. J. Geophys. Res. Biogeosci. 118, 994–1105.

Goulden, M.L., Litvak, M., Miller, S.D., 2007. Factors that control Typha marsh evapotranspiration. Aquat. Bot. 86, 97–106.

Hanis, K.L., Tenuta, M., Amiro, B.D., Papakyriakou, T.N., 2013. Seasonal dynamics of methane emissions from a subarctic fen in the Hudson Bay Lowlands. Biogeosciences 10, 4465–4479.

Heimann, M., Reichstein, M., 2008. Terrestrial ecosystem carbon dynamics and climate feedbacks. Nature 451 (17), 289–292.

Hendriks, D.M.D., van Huissteden, J., Dolman, A.J., van der Molen, M.K., 2007. The full greenhouse gas balance of an abandoned peat meadow. Biogeosciences 4, 411–424.

Herbst, M., Kappen, L., 1999. The ratio of transpiration versus evaporation in a reed belt as influenced by weather conditions. Aquat. Bot. 63, 113–125.

Hommeltenberg, J., Mauder, M., Drosler, M., Heidbach, K., Werle, P., Schmid, H.P., 2014. Ecosystem scale methane fluxes in a natural temperature bog-pine forest in southern Germany. Agric. For. Meteorol. 198–199, 273–284.

IPCC, 2007. Climate Change 2007—The Physical Science Basis, 2007. Contribution of Working Group I to the Fourth Assessment Report of the IPCC. Cambridge University Press, New York.

Irmak, S., Kabenge, I., Rudnick, D., Knezevic, S., Woodward, D., Moravek, M., 2013. Evapotranspiration crop coefficients for mixed riparian plant community and transpiration crop coefficients for Common reed, Cottonwood and Peach-leaf willow in the Platte River Basin, Nebraska-USA. J. Hydrol. 481, 177–190.

Jackowicz-Korczynski, M., Christensen, T.R., Backstrand, K., Crill, P., Friborg, T., Mastepanov, M., Strom, L., 2010. Annual cycle of methane emission from a subarctic peatland. J. Geophys. Res. Biogeosci. 115.

Jacobs, J.M., Mergelsberg, S.L., Lopera, A.F., Myers, D.A., 2002. Evapotranspiration from a wet prairie wetland under drought conditions: Paynes Prairie Preserve, Florida, USA. Wetlands 22 (2), 374–385.

Kayranli, B., Scholz, M., Mustafa, A., et al., 2010. Carbon storage and fluxes within freshwater wetlands: a critical review. Wetlands 30, 111–124.

Lafleur, P.M., 1990. Evapotranspiration from sedge-dominated wetland surfaces. Aquat. Bot. 37, 341–353.

Lai, D.Y.F., 2009. Methane dynamics in northern peatlands: a review. Pedosphere 19, 409–421.

Lei, H.M., Yang, D.W., 2010. Interannual and seasonal variability in evapotranspiration and energy partitioning over an irrigated cropland in the North China Plain. Agric. For. Meteorol. 150, 581–589.

Lenters, J.D., Cutrell, G.J., Istanbulluoglu, E., Scott, D.T., Herrman, K.S., Irmak, A., Eisenhauer, D.E., 2011. Seasonal energy and water balance of a Phragmitesaustralis-dominated wetland in the Republican River basin of south-central Nebraska (USA). J. Hydrol. 408 (1–2), 19–34.

Li, M., Li, W., 2009. Review on Carbon Cycle of Wetland Ecosystem, vol. 28. Huazhong Agric. Univ., pp. 116–123.

Li, Z.Q., Yu, G.R., Wen, X.F., Zhang, L.M., Ren, C.Y., Fu, Y.L., 2005. Energy balance closure at ChinaFLUX sites. Sci. China Ser. D Earth Sci. 48, 51–62.

Limpens, J., Berendse, F., Blodau, C., Canadell, J., Freeman, C., Holden, J., Roulet, N., Rydin, H., Schaepman-Strub, G., 2008. Peatlands and the carbon cycle: from local processes to global implications-a synthesis. Biogeosciences 5, 1475–1491.

Liu, C.Y., Zhou, W.B., 2012. Progress of research on carbon cycle of wetlands in China. Chin. J. Soil Sci. 43, 1264–1270.

Liu, S.M., Xu, Z.W., Wang, W.Z., Jia, Z.Z., Zhu, M.J., Bai, J., Wang, M., 2011. A comparison of eddy-covariance and large aperture scintilla meter measurements with respect to the energy balance closure problem. Hydrol. Earth Syst. Sci. 15, 1291–1306.

Liu, S.M., Xu, Z.W., Zhu, Z.L., Jia, Z.Z., Zhu, M.J., 2013. Measurements of evapotranspiration from eddy-covariance systems and large aperture scintilla meters in the Hai River Basin, China. J. Hydrol. 487 (22), 24–38.

Lloyd, J., Taylor, J.A., 1994. On the temperature dependence of soil respiration. Funct. Ecol. 8, 315–323.

Long, K.D., Flanagan, L.B., Cai, T.B., 2010. Diurnal and seasonal variation in methane emissions in a northern Canadian peatland measured by eddy covariance. Global Change Biol. 16, 2420–2435.

Ma, Y.F., 2015. Estimating Evapotranspiration with Multi-source Remote Sensing Data—A Case Study of Zhangye Desert—Oasis in the Middle Stream of the Heihe River Watershed. Ph.D. Thesis. Beijing Normal Univ., Beijing, China.

Massman, W.J., Lee, X., 2002. Eddy covariance flux corrections and uncertainties in long-term studies of carbon and energy exchanges. Agric. For. Meteorol. 113 (1–4), 121–144.

McDermitt, D.K., Burba, G.G., Xu, L., Anderson, T., Komissarov, A., Riensche, B., Schedlbauer, J., Starr, G., Zona, D., Oechel, W., Oberbauer, S., Hastings, S., 2011. A new low-power, open-path instrument for measuring methane flux by eddy covariance. Appl. Phys. B: Lasers Opt. 102, 391–405.

Nadeau, D.F., Rousseau, A.N., Coursolle, C., Margolis, H.A., Parlange, M.B., 2013. Summer methane fluxes from a boreal bog in northern Quebec, Canada, using eddy covariance measurements. Atmos. Environ. 81, 464–474.

Nnoby, R., 1997. Carbon cycle: inside the black box. Nature 388, 522–523.

Papale, D., Reichstein, M., Aubinet, M., Canfora, E., Bernhofer, C., Kutsch, W., Longdoz, B., Rambal, S., Valentini, R., Vesala, T., Yakir, D., 2006. Towards a standardized processing of net ecosystem exchange measured with eddy covariance technique: algorithms and uncertainty estimation. Biogeosciences 3, 571–583.

Peacock, C.E., Hess, T.M., 2004. Estimating evapotranspiration from a reed bedusing the Bowen ratio energy balance method. Hydrol. Processes 18 (2), 247–260.

Pielke, R.A., 2001. Influence of the spatial distribution of vegetation and soils on the prediction of cumulus convective rainfall. Rev. Geophys. 39, 151–177.

Priban, K., Ondok, J.P., 1985. Heat balance components and evapotranspiration from a sedge-grass marsh. Folia Geobotanica et Phytotaxonomica 20, 41–56.

Raddatz, R.L., Papakyriakou, T.N., Swystun, K.A., Tenuta, M., 2009. Evapotranspiration from a wetland tundra sedge fen: surface resistance of peat for land-surface schemes. Agric. For. Meteorol. 149, 851–861.

Running, S.W., Hunt, E.R., 1993. Generalization of a forest ecosystem process model for other biomes, Biome-BGC, and an application for global scale models scaling processes between leaf and landscape level. In: Ehleringe, J.R., Field, C.B. (Eds.), Scaling Physiological Process: Leaf of Globe. Academic Press, San Diego, pp. 141–158.

Runkle, B.R.K., Wille, C., Gažovič, M., Wilmking, M., Kutzbach, L., 2014. The surface energy balance and its drivers in a boreal peatland fen of northwestern Russia. J. Hydrol. 511 (16), 359–373.

Saito, M., Miyata, A., Nagai, H., Yamada, T., 2005. Seasonal variation of carbon dioxide exchange in rice paddy field in Japan. Agric. For. Meteorol. 135 (1–4), 93–104.

Schedlbauer, J.L., Oberbauer, S.F., Starr, G., Jimenez, K.L., 2011. Controls on sensible heat and latent energy fluxes from a short-hydroperiod Florida Everglades marsh. J. Hydrol. 411, 331–341.

Shukla, J., Mintz, Y., 1982. Influence of land-surface evapotranspiration on the Earth's climate. Science 215, 1498–1501.

Sun, L., Song, C., 2008. Evapotranspiration from a freshwater marsh in the Sanjiang Plain, Northeast China. J. Hydrol. 352 (1–2), 202–210.

Sun, G., Sun, J.X., Zhou, G.S., 2009. Water and carbon dynamics in selected ecosystems in China. Agric. For. Meteorol. 149, 1789–1790.

Sun, G., Alstad, K., Chen, J.Q., Chen, S.P., Ford, C.R., Lin, G.H., Liu, C.F., Lu, N., McNulty, S.G., Miao, H.X., Noormets, A., Vose, J.M., Wilske, B., Zeppel, M., Zhang, Y., Zhang, Z.Q., 2011. A general predictive model for estimating monthly ecosystem evapotranspiration. Ecohydrology 4, 245–255.

Tanner, B.D., Greene, J.P., 1989. Measurements of Sensible Heat Flux and Water Vapor Fluxes Using Eddy Correlation Methods, Final Report to US Army Dugway Proving Grounds, Utah, USA, DAAD 09-87 D-0088.

Thornton, P.E., Running, S.W., 1999. An improved algorithm for estimating incident daily solar radiation from measurements of temperature humidity, and precipitation. Agric. For. Meteorol. 93, 211–228.

Thornton, P.E., 1998. Description of a Numerical Simulation Model for Predicting the Dynamics of Energy, Water, Carbon and Nitrogen in a Terrestrial Ecosystem. Ph.D. Thesis. University of Montana, Missoula, USA.

Twine, T.E., Kustas, W.P., Norman, J.M., Cook, D.R., Houser, P.R., Meyers, T.P., Prueger, J.H., Starks, P.J., Wesely, M.L., 2000. Correcting eddy-covariance flux underestimates over a grassland. Agric. For. Meteorol. 103, 279–300.

Wang, H.S., Jia, G.S., Fu, C.B., Feng, J.M., Zhao, T.B., Ma, Z.G., 2010. Deriving maximal light use efficiency from coordinated flux measurements and satellite data for regional gross primary production modeling. Remote Sens. Environ. 114 (10), 2248–2258.

Whalen, S.C., 2005. Biogeochemistry of methane exchange between natural wetlands and the atmosphere. Environ. Eng. Sci. 22, 73–94.

Wille, C., Kutzbach, L., Sachs, T., Wagner, D., Pfeiffer, E.M., 2008. Methane emission from Siberian arctic polygonal tundra: eddy covariance measurements and modeling. Global Change Biol. 14, 1395–1408.

Xiao, J.F., Sun, G., Chen, J.Q., Chen, H., Chen, S.P., Dong, G., Gao, S.H., Guo, H.Q., Guo, J.X., Han, S.J., Kato, T., Li, Y.L., Lin, G.H., Lu, W.Z., Ma, M.G., McNulty, S., Shao, C.L., Wang, X.F., Xie, X., Zhang, X.D., Zhang, Z.Q., Zhao, B., Zhou, G.S., Zhou, J., 2013. Carbon fluxes, evapotranspiration, and water use efficiency of terrestrial ecosystems in China. Agric. For. Meteorol. 182–183, 76–90.

Xu, S., Ma, T., Liu, Y., 2011. Application of a multi-cylinder evapotranspirometer method for evapotranspiration measurements in wetlands. Aquat. Bot. 95, 45–50.

Xu, Z.W., Liu, S.M., Li, X., Shi, S.J., Wang, J.M., Zhu, Z.L., Xu, T.R., Wang, W.Z., Ma, M.G., 2013. Intercomparison of surface energy flux measurement systems used during the HiWATER—MUSOEXE. J. Geophys. Res. D: Atmos. 118 (13), 140–157.

Yao, W., Han, M., Xu, S.G., 2010. Estimating the regional evapotranspiration in Zhalong wetland with the Two-Source Energy Balance (TSEB) model andLand-sat7/ETM+ images. Ecol. Inform. 5, 348–358.

Zhang, L., Sun, R., Xu, Z.W., Qiao, C., Jiang, G.Q., 2015. Diurnal and seasonal variations in carbon dioxide exchange in ecosystems in the Zhangye oasis area, northwest China. PLoS One, http://dx.doi.org/10.1371/journal.pone.0120660.

Zhou, L., Zhou, G.S., 2009. Measurement and modelling of evapotranspiration over areed (*Phragmites australis*) marsh in Northeast China. J. Hydrol. 408 (1–2), 19–34.

Zhu, Z.L., Sun, X.M., Wen, X.F., 2006. Study on the processing method of nighttime $CO_2$ eddy covariance flux data in ChinaFLUX. Sci. China Ser. D Earth Sci. 49 (Suppl. II), 36–46.